# A Mode Propagation Database Suitable for Code Validation Utilizing the NASA Glenn Advanced Noise Control Fan and Artificial Sources

Daniel L. Sutliff[*],

*NASA Glenn Research Center*

*21000 Brookpark Road, Cleveland, OH 44135*

**The NASA Glenn Research Center's Advanced Noise Control Fan (ANCF) was developed in the early 1990s to provide a convenient test bed to measure and understand fan-generated acoustics, duct propagation, and radiation to the farfield. A series of tests were performed primarily for the use of code validation and tool validation. Rotating Rake mode measurements were acquired for parametric sets of: (i) mode blockage, (ii) liner insertion loss, (iii) short ducts, and (iv) mode reflection.**

## I.   Introduction

THE NASA Glenn Research Center (GRC) has been involved in several programs (Advanced Subsonic Technology, Quiet Aircraft Technology, and the Fundamental Aeronautics Subsonic Fixed Wing) whose goals were the reduction in transport aircraft noise attributed to the turbofan engine. A component of turbofan noise[1] is the fan noise caused by rotor-stator, and other interactions, coupled to duct propagation that radiates to the farfield. computational aero-acoustic (CAA) codes and unique measurement tools are required to enable the development of noise reduction technologies. In order to validate these codes and tools, it is necessary to have an acoustic database.

Parametric studies were performed for several conceptual representations: (i) mode blockage due to stator vanes or rotor blades, (ii) liner insertion loss, (iii) the effects of short ducts on radiation, and (iv) mode reflection due to duct terminations. The intent is not to document specific cases as relevant to a modern turbofan but to provide a database for code validation. Nor will a significant portion of the data be presented, but rather limited samples. The database was acquired on the Advanced Noise Control Fan[2,3] (ANCF) test bed that was built in the early 1990s[4,5] to evaluate noise reduction concepts and to provide databases for CAA code validation. Figure 1 shows the Aero-Acoustic Propulsion Laboratory where the ANCF is located and Figure 2 is a photo of the ANCF.

A Configurable Fan Artificial Noise System (CFANS) was utilized to generate and control circumferential modes (*m*). The system consists of 4 axially distributed rows, each with 16 circumferentially distributed sets of electromagnetic drivers flush mounted on the inner wall. There are two spool pieces, each having 2 driver rows (see figure 3). A Labview[TM] program is used to generate the waveforms sent to each driver independently, in the proper phase relationship to generate the desired circumferential mode. The signals to each row can be adjusted globally to effect the radial distribution, if desired. The practical limits of the system are |m-order| $\leq$ 7, and frequency $\leq$ 1500 Hz. Figure 4 shows the typical high quality output from the CFANS for a sample case where mode *m*=2 was the target mode generated. The upper row of 3-D "tombstone" plots is at 480 Hz (equivalent to BPF on ANCF) and the lower row is for 960 Hz (equivalent to 2BPF). The two columns represent data from two different builds (limited teardown and reassembly, about one month apart) for a limited repeatability demonstration. The target mode is at least 20 dB above any other individual mode, and mostly 10 dB above the sum of all other extraneous modes. This is shown in the small bar graph above and to the right of the 3-D plot. The repeatability (admittedly limited) is within a dB. Table I provides the modes generated and their cut-off ratios for several hub-to-tip ratios ($\sigma$) inside the duct, for the studies documented in this paper. The modes were measured by the Rotating Rake mode measurement system mounted at the duct radiation plane. The Rotating Rake[6] system was developed and implemented by the NASA Glenn Research Center in the 1990s to measure turbofan duct acoustic modes. The system is a continuously rotating radial microphone rake that is inserted into the duct. It provides a complete map of the acoustic duct modes present
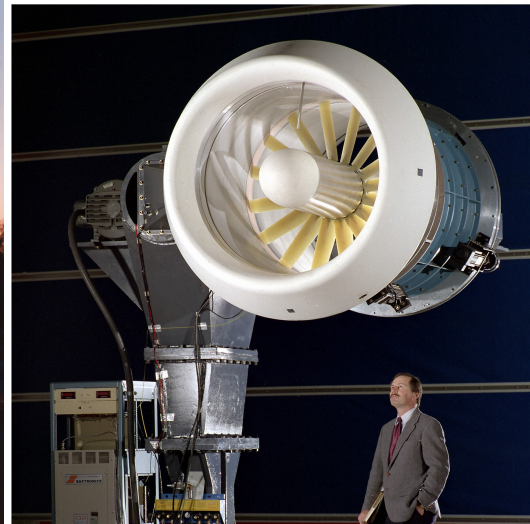
---

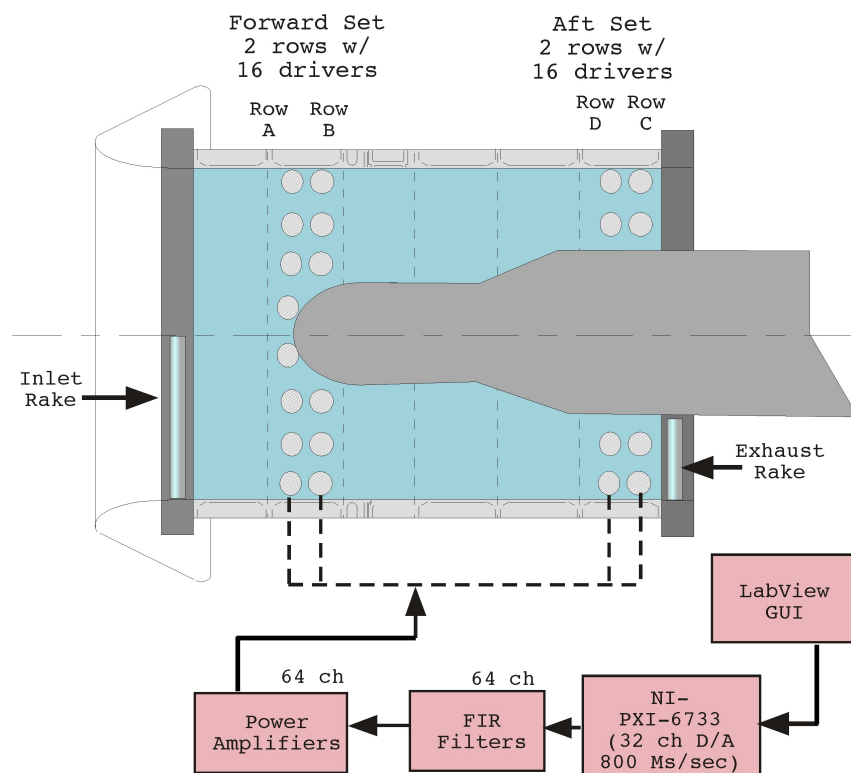[*]Aerospace Engineer, Acoustics Branch, MS 54-3

in a ducted fan. The schematics call out the location of the rotating rake measurement locations(s), generally at the duct inlet or exit planes. Figure 5 shows the propagation angles that are referenced in the relevant sections.


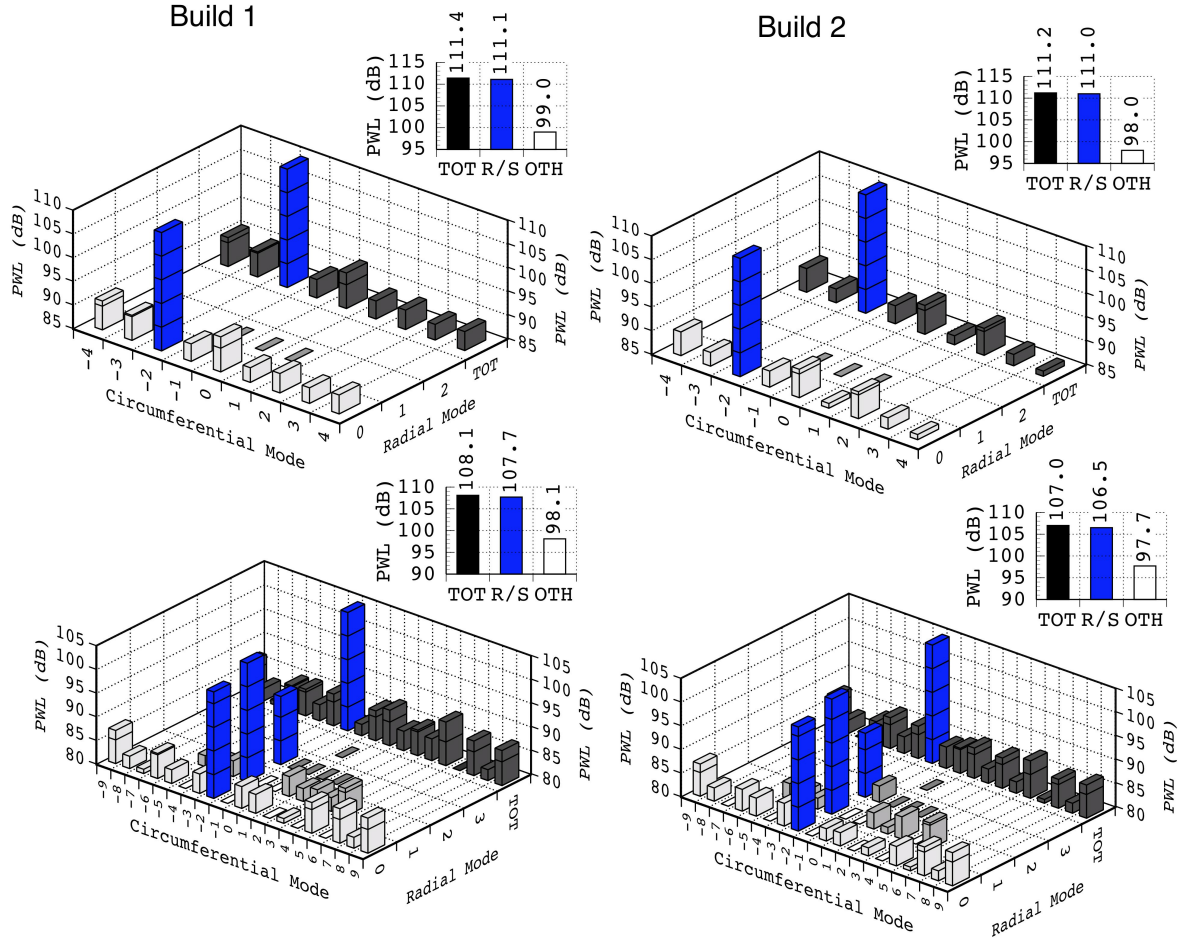
**Figure 1. Aero-Acoustic Propulsion Laboratory**



**Figure 2. Advanced Noise Control Fan**



**Figure 3. Schematic of Configurable Fan Artificial Noise System**

**480Hz \* Mode 2** (Build 1 and Build 2)

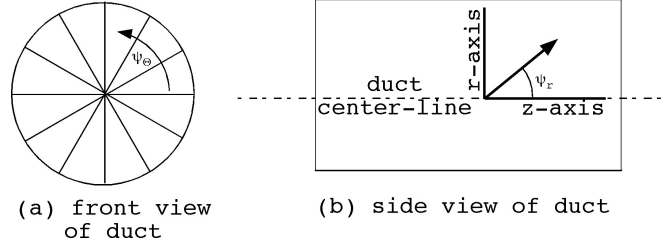**960Hz \* Mode 2** (Build 1 and Build 2)

TOT —  Total Power in Harmonic (all modes)
R/S — Power in Rotor/Stator Interaction Mode
OTH — Power in other modes (non-R/S modes)

**Figure 4. Sample Output of Configurable Fan Artificial Noise System**

**TABLE I: Modes Generated for Parametric Studies using CFANS**

| FREQ (Hz) | MODES | INLET (σ=0.0) | CUT-OFF RATIOS (σ, hub-to-tip ratio) R/S (σ=.375) | EXHAUST (σ=0.5) |
|---|---|---|---|---|
| 480 | +/-(2,0) | 1.77 | 1.89 | 2.01 |
| "" | +/-(4,0) | 1.02 | 1.03 | 1.04 |
| | | | | |
| 580 | +(2,0) | 2.14 | | |
| 600 | +(2,0)/(2,1) | 2.21/1.01 | | |
| 700 | +(2,0)/(2,1) | 2.58/1.17 | | |
| 880 | +(2,0)/(2,1)/(2,2) | 3.24/1.48/0.99 | | |
| | | | | |
| 960 | +/-(2,0)/(2,1)/(2,2) | 3.54/1.61/1.08 | 3.79/1.72/1.02 | 4.03/1.53/- |
| "" | +/-(4,0)/(4,1) | 2.03/1.16 | 2.06/1.22 | 2.09/1.22 |
| "" | +/-(6,0) | 1.44 | 1.45 | 1.45 |

American Institute of Aeronautics and Astronautics

(a) front view of duct    (b) side view of duct

**Figure 5.  Schematic of ANCF in Blockage Configurations**

## II.   Mode Blockage

### A.  Setup

The objective of this portion of the test was to obtain the effect of geometrical obstructions on mode propagation i.e. blockage (or transmission loss). Blockage effects were measured separately for stationary geometry (stator vanes) or for rotating geometry (fan blades). In order to provide a larger database, and taking advantage of the flexibility inherent in a no-flow condition, the existing ANCF stator vanes were pitched at a range of angles. Geometry of fixed 3-D surfaces prevented pitching the stator vanes a full 90°, therefore the tip gap was increased to allow for this rotation. The center-body was retained, creating a transition from $\sigma$=0 at the inlet to $\sigma$ =0.5 at the exhaust exit plane. These configurations are shown schematically in figure 6 and pictorially in figure 7.

The baseline case was a clean duct, with no stator vanes or fan blades. A parametric set of modes (Table I) were generated at either the forward or aft driver set, and measured by the opposite rotating rake. That is: modes generated by the forward driver set were measured by the exhaust rake; modes generated by the aft driver set were measured by the inlet rake. Fourteen or twenty-eight stator vanes were installed at various pitch angles (Table II) and the rake mode measurements repeated. Separately, the rotor blades were installed at 3 different pitch angles. The nominal pitch angle for ANCF is 28° and that configuration was run at 3 different fan speeds. The fan pitch angle was changed by +/-10° and run at a single fan speed for those two angles.

The assumption is made that the source does not change so that the blockage can be computed by subtracting the mode PWL measured with stators installed from the mode PWL measured in the clean configuration (either with flow or without flow). The configurations were tested over a period of several weeks whereby the ambient temperature varied by 10° F. The mode frequencies generated were at constant frequency, corrected to standard day (59 °F). Note that this is standard for duct propagation, but does not take into account any changes in the driver response due to changes in actual driver frequency.

### B.  Results

The blockage is defined as the mode amplitude measured by the rotating rake with the duct in the clean configuration minus the mode amplitude measured with the desired blockage installed between the source and the rake. Thus, a positive number indicates the mode amplitude has been reduced due to blockage.

Figure 8 shows the results for mode blockage at various stator vane configurations for modes at 480 and 960 Hz. The blockage for the forward propagating direction (generated by the aft drivers, propagation through the obstruction, and measured by the inlet rake) is shown in figure 8a (480 Hz) and 8b (960 Hz).

The case labeled clean is actually the difference between two clean cases several weeks apart. As such it can provide an estimate of the significance for a measured blockage value. This number is about +/-1 dB. Anything less than that cannot be assumed to be a result relevant to blockage.

Little blockage is seen at low m-orders in either direction. These modes' circumferential propagation angles are relatively low as a result of their higher cut-off ratio. The higher order circumferential modes (4 at 480 Hz, 6 at 960 Hz) are significantly blocked as a result of their higher circumferential propagation angles ($\Psi_\theta$) – see figure 5a. The stator vane count is seen to increase the mode blockage levels. Thus, it appears as if projected area is the biggest influence on blockage levels under these conditions.
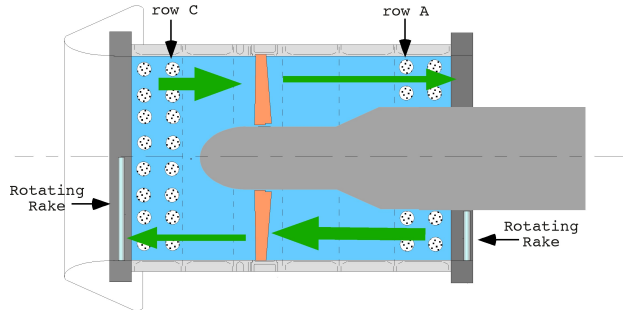
Blockage levels obtained with the rotor (alone) at various rotor RPM ($\Omega$) and pitch angles ($\alpha$) are shown in figure 9.
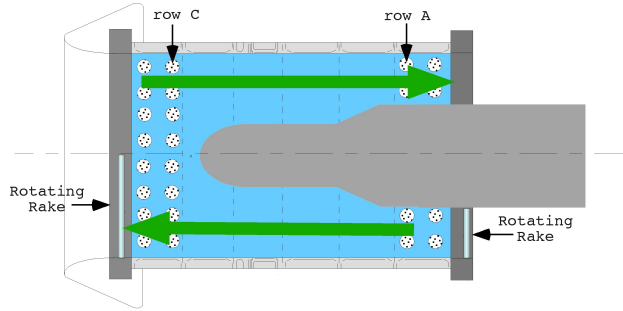
**(a) Clean Duct**
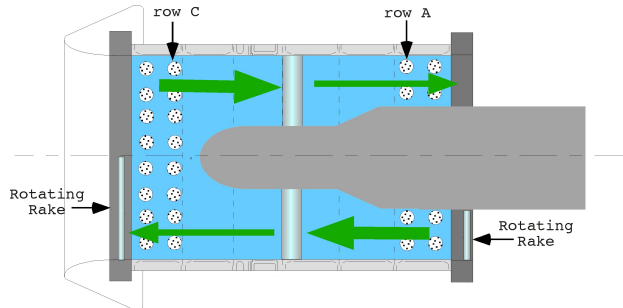
Modes generated by driver spools are measured at opposite rake.

Assumption is source does not change with the insertion of blockage or the addition of flow.



**(b) Stationary Blockage**

**TABLE II: Blockage Configurations Tested**

(a) STATOR VANE CONFIGS:

| 14 VANES | 28 VANES |
|---|---|
| --- | α=20° |
| α=45° | α=45° |
| α=45°~ δ=1.63" | α=45°~ δ=1.63" |
| α=90°~ δ=1.63" | --- |

Designation: Pitch Angle (α) ~ tip gap (δ)

(b) FAN BLADE CONFIGS:

θ=18° (1800 Ω)
θ=28° (0, 900, 1800 Ω)
θ=38° (900 Ω)



**(c) Rotating Blockage**

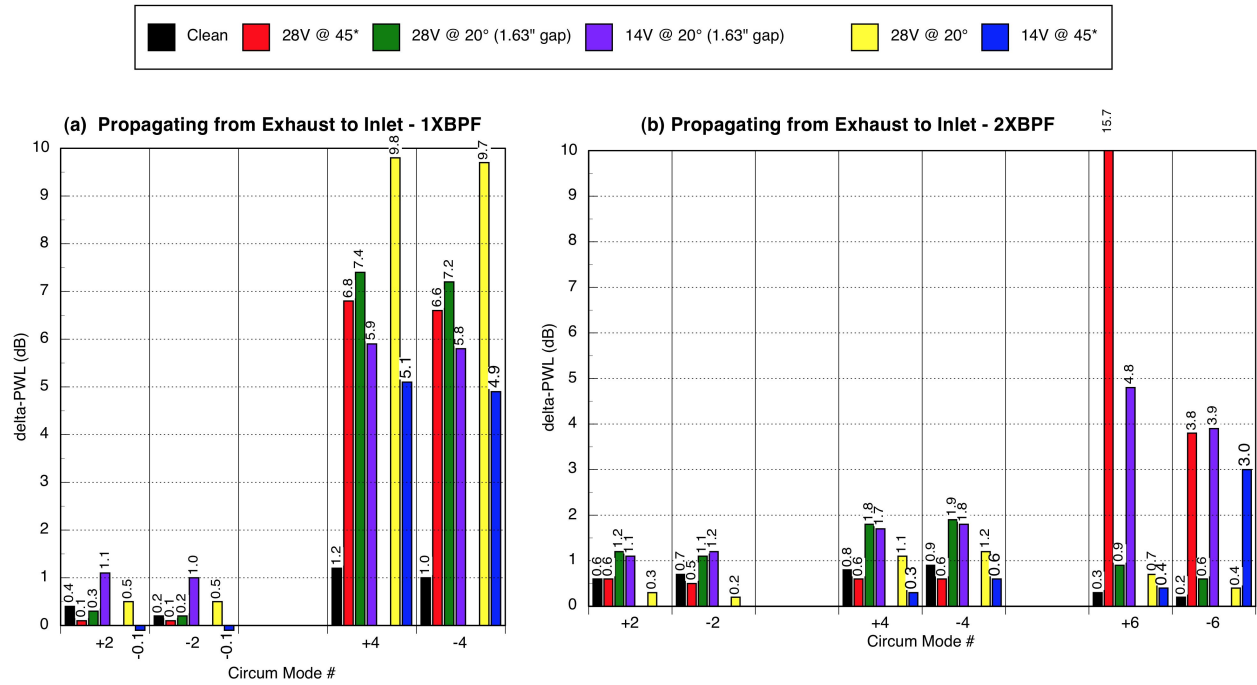**Figure 6.  Schematic of ANCF in Blockage Configurations**
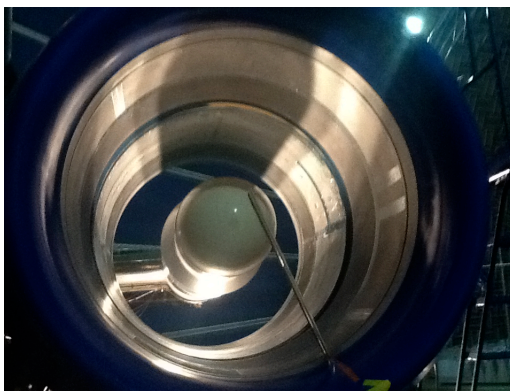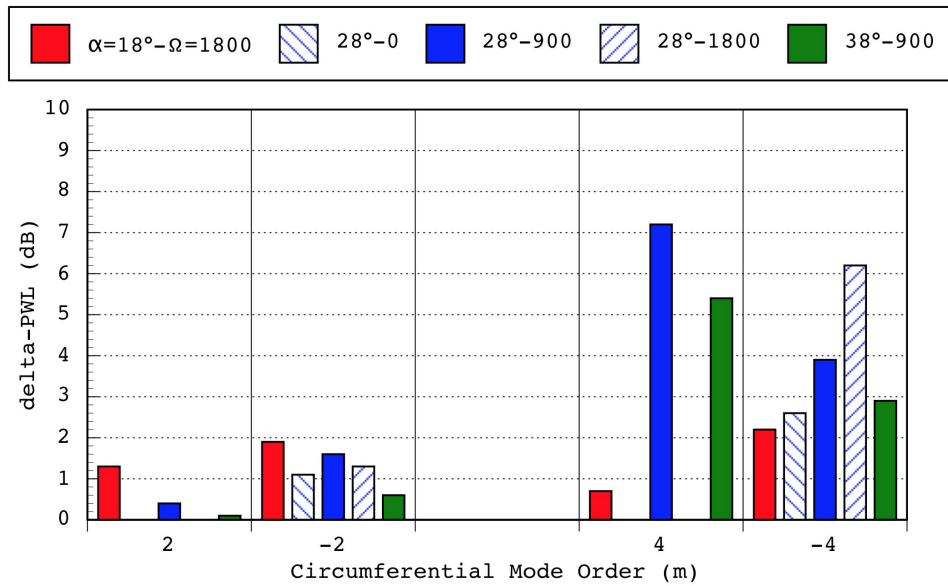


**a. Clean Duct Configuration**  **b. 28 Vane – 45° Pitch Configuration**

**Figure 7.  Photos of ANCF in Mode Blockage Configurations**

**Figure 8. Circumferential Mode Blockage Levels from Stator Vanes**



**Figure 9. Circumferential Mode Blockage Levels from Rotor Vanes**

American Institute of Aeronautics and Astronautics

# III. Liner Evaluation

## A. Set-up

Figure 10 shows the schematic of the ANCF configuration for the evaluation of insertion loss due to a liner. The liner used was a single-degree-of-freedom (SDOF) liner with a screen mesh on a 34 percent-open-area (POA). The normalized design resistance for the liner is 1.7ρc. The liner core depth is 0.85"; resonance frequency is 3221 Hz.

The rotating rake ring was installed in one of two locations: upstream (figure 10a) of the liner to measure the modal PWL at the entrance, and downstream (figure 10b) of the liner to measure the modal PWL at the liner exit. Comparing the two results in liner insertion loss (positive number indicates attenuation). These rake configurations were tested for both the liner exposed and taped over (to provide a hard-wall baseline).

## B. Results

Figure 11 shows the mode PWLs measured at the entrance and the exit for the hard-wall and the liner. Figure 11a shows that at BPF the insertion loss is minor – not surprising as this frequency was not the design frequency. Note that in general the comparison of the mode strength at the entrance to the HW is comparable to the mode strength at the entrance of the liner. An exception is that mode 4 HW to SW entrance comparison shows a huge variation in PWL. This is thought to be due to being close to cut-off and being more susceptible to reflections. Figure 11b shows the insertion loss at 960 Hz, near the target design of the liner. The attenuation is much greater, and increases as the mode number increases. This is expected as the higher mode numbers have lower cut-off ratios – it is generally accepted that liners are more effective at cut-off ratios near unity[7] since the mode angle is propagating into the liner (see figure 5b).
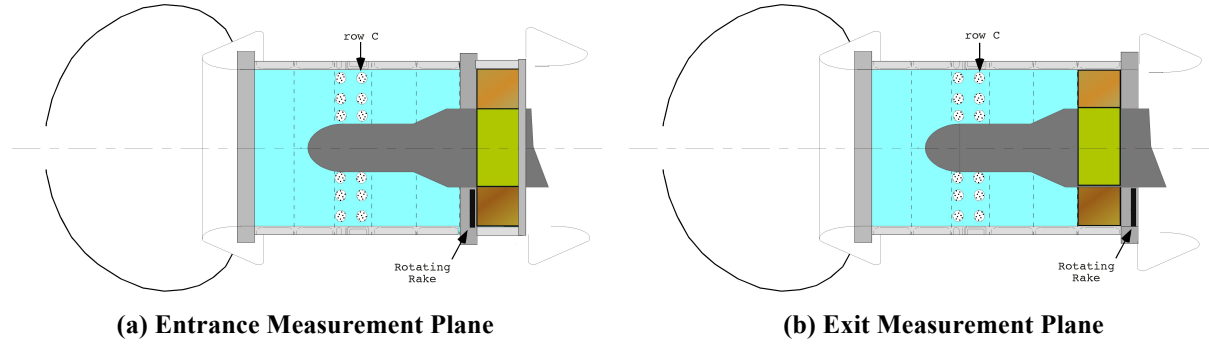


(a) Entrance Measurement Plane     (b) Exit Measurement Plane

**Figure 10. Schematic of Liner Configurations Tested**



(a) 480 Hz                          (b) 960 Hz
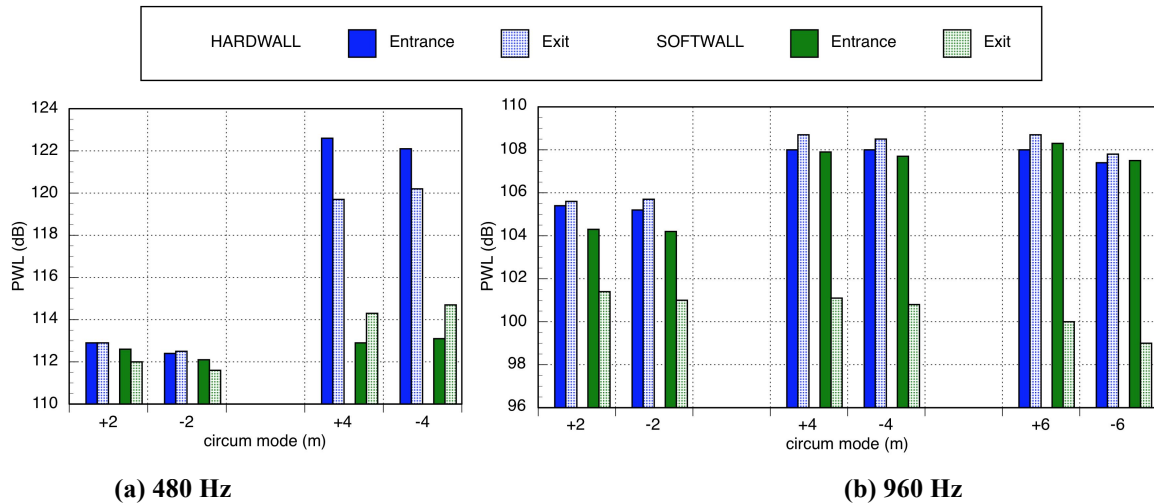
**Figure 11. Liner Configurations Results**

American Institute of Aeronautics and Astronautics

## IV.  Short-Duct Effects

Duct mode propagation theory assumes a long duct as defined by the Length to Diameter ratio (L/D > 1) in order for the classic mode structure to develop along the predicted analytical forms. In reality, even a cut-off mode can be said to "propagate" from the source, albeit at a significant decay rate. Modes that are well below cut-on may decay at a rate of 80-100 dB per duct diameter, while a mode just below cut-on may decay at a rate of only 2-3 dB per diameter[8].

### A.  Set-up

To investigate this effect, the ANCF/CFANS was tested in two duct lengths, with the actuated driver row 1 diameter from the duct exit, and 1/4–diameter from the duct exit (figure 12). The modes were measured at the inlet entrance plane. The duct exit was filled with absorptive material to prevent reflections as well as farfield contamination from duct aft radiation. For this portion of the test, corresponding far-field directivity data were acquired. The farfield array was kept at a constant distance from duct inlet entrance plane.

### B.  Results

Typical in-duct mode results for the two duct lengths are shown in Figure 13. The generated mode was m=+2 or m=-2. Figure 13a shows the modal decomposition. For the long duct all of the "extraneous" modes have decayed to the measurement floor ~ 75-80 dB. The modes in the short duct configuration have not decayed, nearly equal in strength to the target mode. Figure 13b illustrates this by comparing the total PWL in all modes, PWL in the generated mode, and the sum of the non-target mode. For the long duct the majority of the power is in the target mode, for the short duct the extraneous modes carry more energy.

The effect in the far-field indicates that the modes measured at the inlet plane do in fact propagate to the farfield. Figure 14 shows the tonal directivity for m=+/-2. The long duct directivity shows the characteristic flat lobe associated with a well cut-on mode. Note the symmetry between the positive and negative mode. The pattern radiated from the short duct shows significant departure from the classical directivity. It also shows an asymmetry between the positive and negative generated mode. These effects are due to axisymmetric variation[9] resulting from multiple modes.
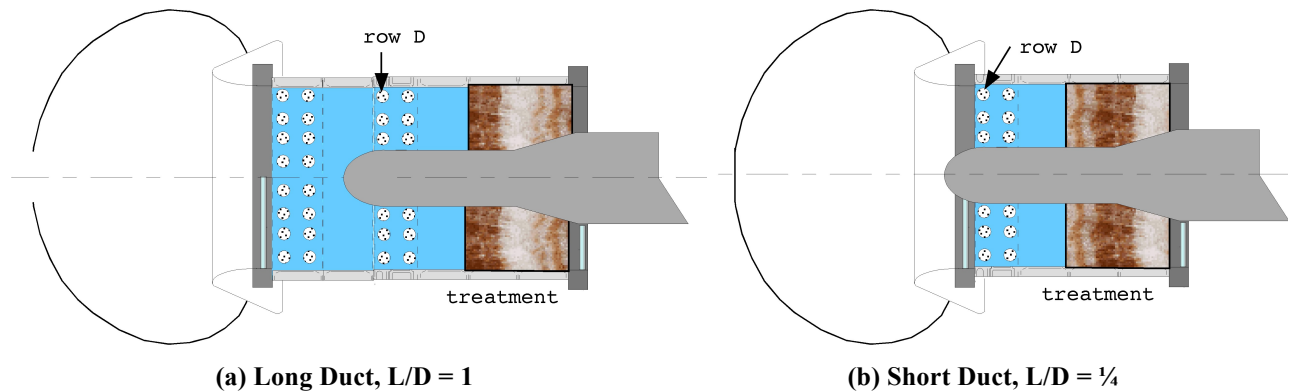


(a) Long Duct, L/D = 1                    (b) Short Duct, L/D = ¼

**Figure 12. Effect of Duct Length on In-Duct Modes**

**(a) Individual Modes**

**(b) Modal Summation**
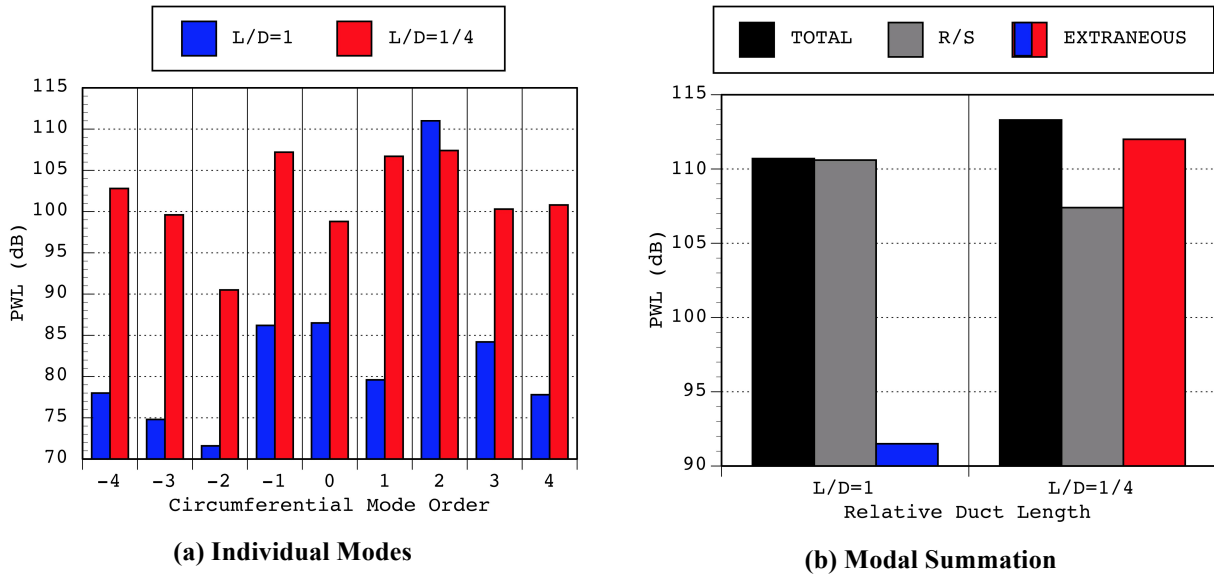
**Figure 13. Effect of Duct Length on In-Duct Modes**
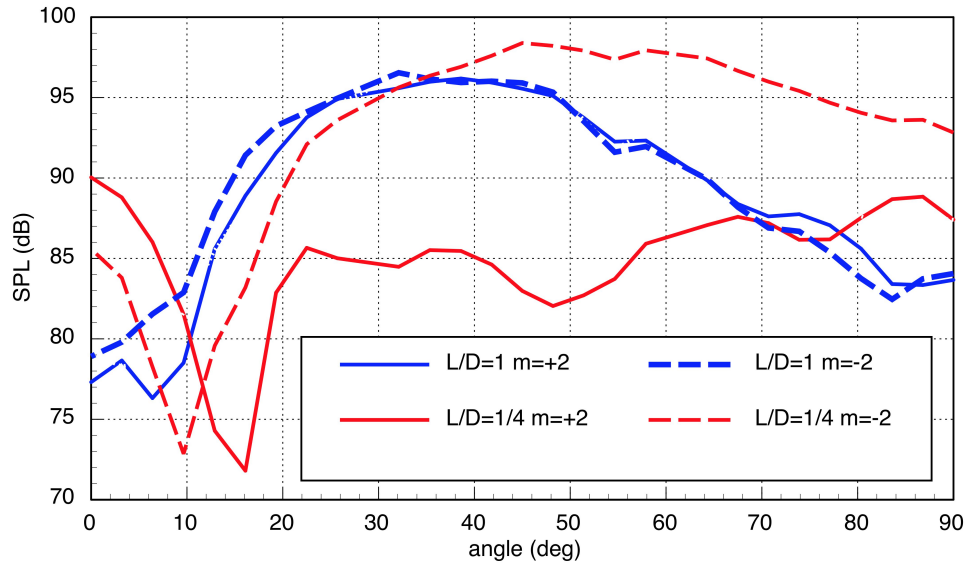


**Figure 14. Effect of Duct Length on Far-field Directivity**

American Institute of Aeronautics and Astronautics

# V. Mode Reflection

## A. Setup

In order to provide a clean, cylindrical duct, for this experiment the ANCF was built up off of the stanchion that normally supports the fan and duct sections that make up the nacelle. That is, the spool pieces were stacked up in a vertical orientation based on the floor. This removed center-body and support pylon from the arrangement, providing a constant area cylindrical duct. Two configurations were tested in this setup: (a) with the flow lip attached, and (b) without the flow lip attached, which left a bare flange as the exit termination. (Figures 15 and 16.) The entire stack rested on the floor, and approximately 6" of foam material was placed in the bottom of the stack to minimize reflections from the floor.

Typically, a single rake, extending from the outer-wall to the duct centerline, has been mounted to measure duct modes. It has been known[10,11] that measuring at a single axial location will not be able to account for reflections in the duct, therefore, for this experiment an additional rake was mounted on the same rotating ring as the original. This 2nd rake was adjustable in the axial direction over the range of 2.5" to 10.5", in fixed, one-inch increments, and was mounted 180° in the circumferential direction from the original rake, which remains fixed in the axial direction. Figures 17a and 17b show this arrangement.

Data were acquired from the dual rakes in order to provide the two-point axial variation needed to compute the reflection. Reflections were created using two methods. The first method relies on the natural reflections due to an open-ended exit termination. The ring containing the dual rotating rake system was mounted at the exit of the ANCF stack-up (figure 15a). The single driver row (C) farthest from the exit termination was used to generate the modes in Table I. This configuration was run with the flow lip attached – this was assumed to minimize reflections, and with the flow lip removed, creating a sharp 90° flanged exit – this was assumed to create reflections. A second configuration was used to generate artificial reflections, see Figure 15b. This was accomplished by locating the dual rake ring in the center of the stack-up. Driver row C was used to generate the "primary" wave and driver set B was used to generate the "reflected" wave. Each driver row was actuated independently and the modes were measured by the dual rakes. Then both sets were activated simultaneously and the resulting superposition was measured.

The concept is that the measured combination $\overline{B+C}$ is the resulting superimposed mode and is equal to $B+C$ measured independently and mathematically combined. Thus any technique to separate the "primary" from the "reflected" wave will result in $B$ and $C$ that can be compared to the independent measurements for code validation. ($B$ and $C$ are arbitrary amplitudes generated by driver rows B & C) This assumes that there are no other reflections, either from the duct exit, the anechoic termination, or the rakes themselves. It also assumes that the driver rows generate the same mode PWL (magnitude and phase) independently and when combined. It also assumes that the rake response is independent of the mode propagation direction.

## B. Results

The dual rake measurements were evaluated to determine if the basic assumptions were correct. Data from each rake were acquired when installed separately, in each of the two circumferential locations, in a reverse orientation, and with both rakes installed so that the adjustable upstream rake blocked the fixed rake. Table III shows these results. In general the results agree to within a dB.

Figure 18 shows typical results from the dual rake measurements. The fixed rake mode PWLs are compared to the adjustable rake levels as a function of separation distance. Figure 18a is data at 480 Hz where a single radial mode is cut on; figure 18b shows data at 960 Hz where 3 radial modes are cut-on. The flow-lip on and flow-lip off cases are compared. The data show that the mode PWL variation in axial distance is greater with the flow-lip removed, indicating a stronger reflection, due to constructive and destructive interference, as expected. Note also that the fixed rake measurements are constant as the movable rake is adjusted (also as expected).

Figure 18c shows a sample of the data from the dual-row configuration. In this sample, $m$=2 was generated and the rakes were separated axially by 6.5". The amplitude of driver row C was held constant. The amplitude of driver row B was varied to simulate variation of the strength of the "reflection" from 1.0 to 0.25. This is indicated on the plot by "G"; the ratio of the driver row B amplitude to driver row C amplitude. The mode PWL from each row actuated alone and together is presented. Variations in the sum $\overline{B+C}$ are seen as the strength of the artificially generated reflection is modified.
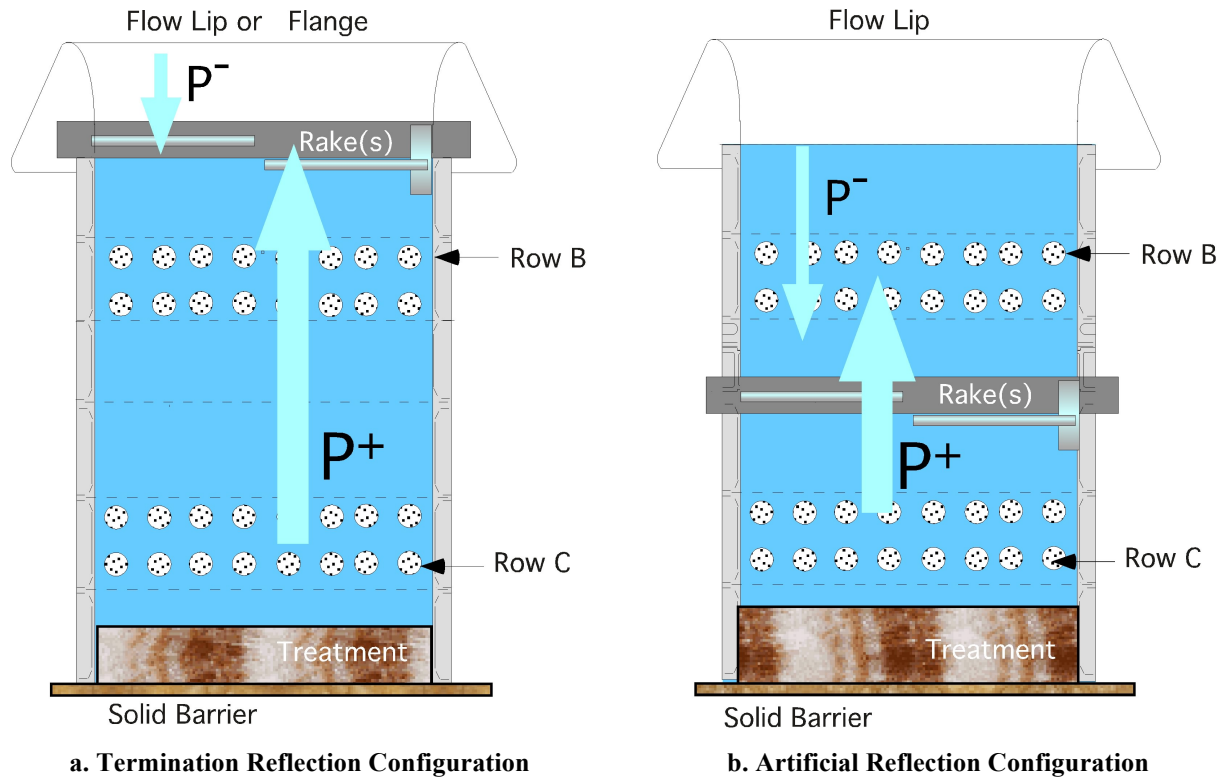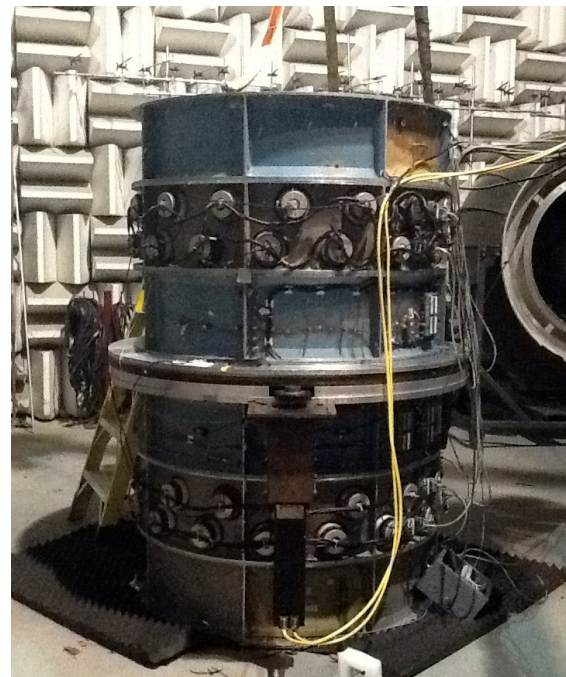
**a. Termination Reflection Configuration**     **b. Artificial Reflection Configuration**

**Figure 15.  ANCF in Mode Reflection Configurations**
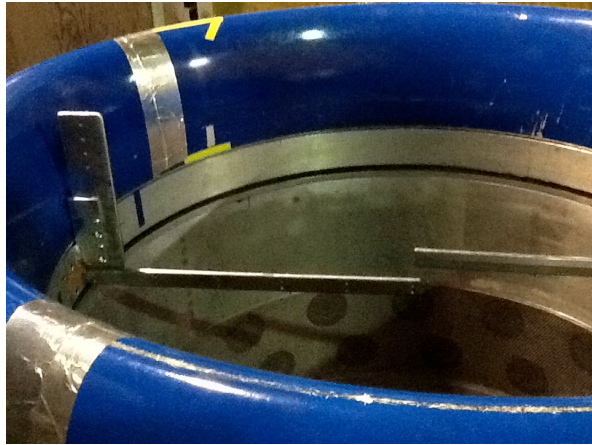


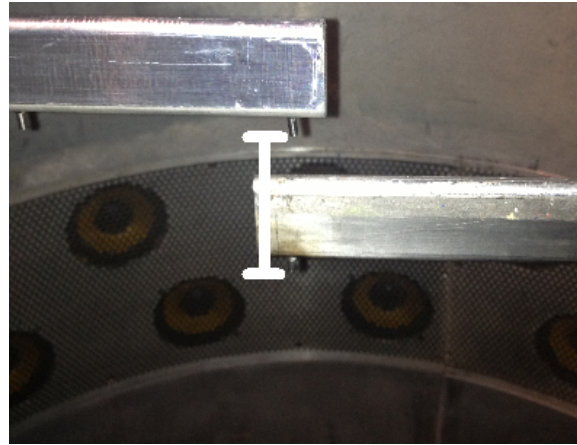**a. with flow lip attached**                    **b. with flow lip removed**

**Figure 16. ANCF in Off-Stanchion Configuration**

a. 2<sup>nd</sup> Rotating Rake w/ Extensions     b. Close-up of Rotating Rake Separation

**Figure 17. Dual Rakes on Same Rotating Ring**

**TABLE III.  Mode PWLs for a Range of Modes, Frequencies, and Rake Orientations.**

| PWL in dB | Fixed Rake 0° Position Standard Orientation | Fixed Rake 180° Position Standard Orientation | Fixed Rake 0° Position Reverse Orientation | Extended Rake 180° Position Standard Orientation | Fixed Rake Blocked 0° Position Standard Orientation |
|---|---|---|---|---|---|
| **1BPF** | | | | | |
| **(2,0)** | 116.5/116.2 | 116.9/116.8 | 116.6 | 116.1 | 116.1 |
| **(4,0)** | 99.1/98.1 | 98.7/98.0 | 98.1 | 98.9 | 98.2 |
| **2BPF** | | | | | |
| **m=2** | 113.7/113.3 | 113.0/113.3 | 113.5 | 112.7 | 113.3 |
| **(2,0)** | 106.0/105.6 | 105.7/105.6 | 105.2 | 105.1 | 105.5 |
| **(2,1)** | 108.5/107.7 | 107.3/107.2 | 108 | 106.4 | 107.8 |
| **(2,2)** | 110.9/110.8 | 110.4/111.0 | 111 | 110.5 | 110.8 |
| **m=4** | 112.9/112.3 | 112.3/112.3 | 112.3 | 111.8 | 112.4 |
| **(4,0)** | 109.2/108.4 | 108.8/108.8 | 108.3 | 108 | 108.5 |
| **(4,1)** | 110.4/110.0 | 109.7/109.8 | 110.1 | 109.4 | 110.2 |
| **(6,0)** | 113.7/112.4 | 112.9/112.9 | 113.2 | 112.3 | 112.7 |

American Institute of Aeronautics and Astronautics
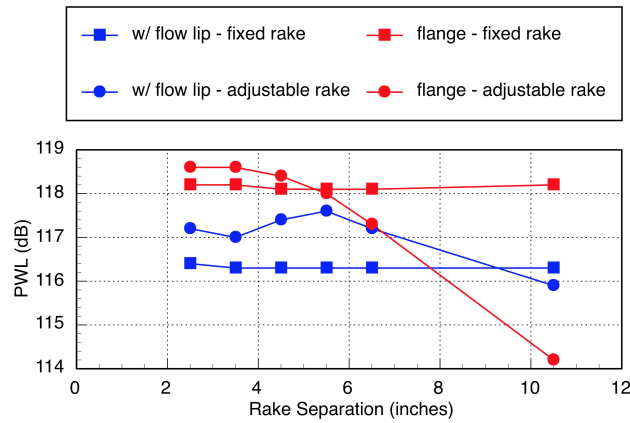
**(a) 480 Hz – Termination Reflection**
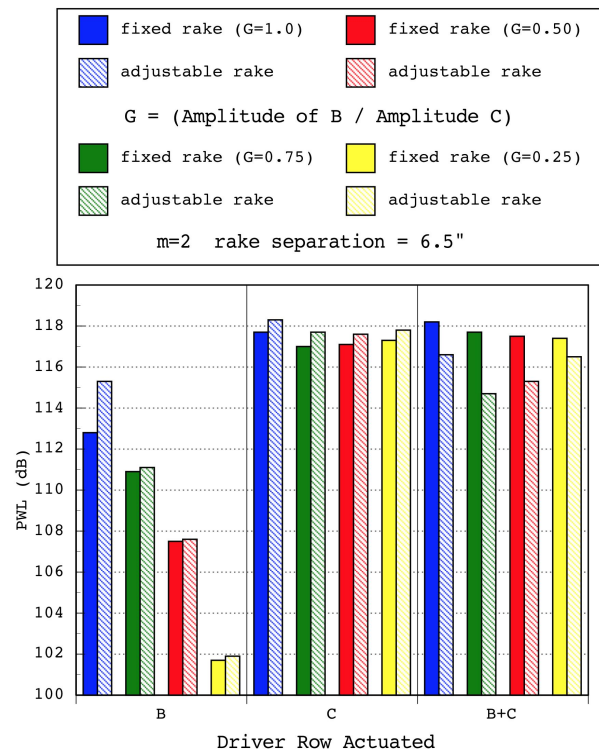


**(c) 480 Hz– Artificial Reflection**
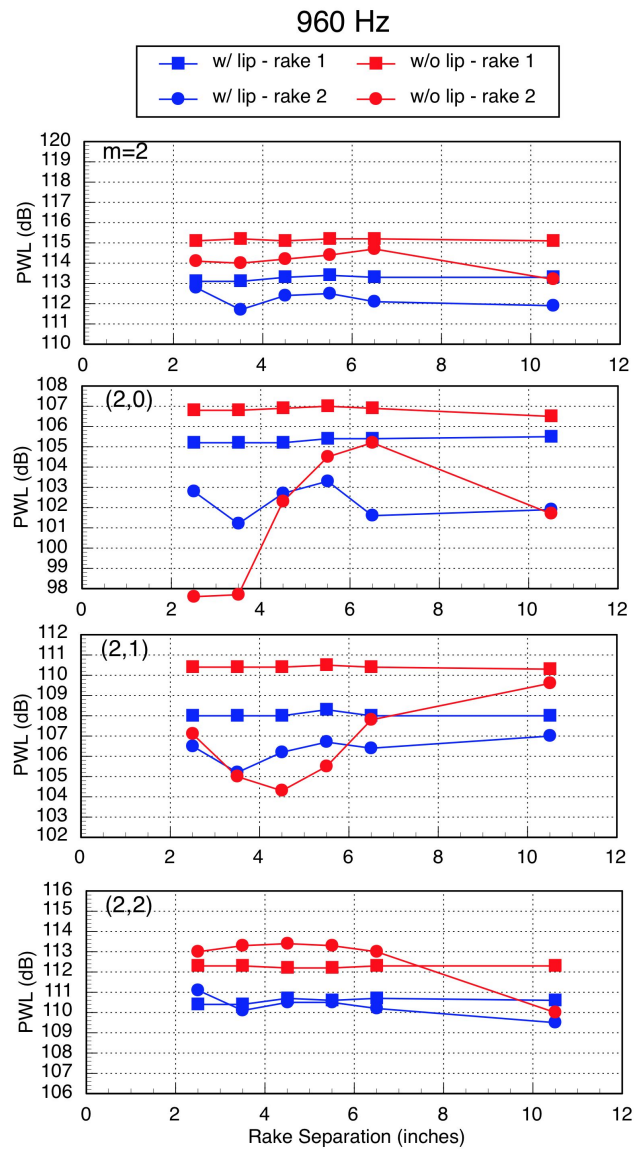


**(b) 960 Hz– Termination Reflection**

**Figure 18.  Changes in Mode Levels with Axial Distance (*m*=+2)**

## VI.  Conclusion

Parametric sets of mode propagation databases were acquired for the purpose of computational aero-acoustic and acoustic measurement tool validation. Limited samples of the data were presented and analysis limited to ensuring the database is valid relative to basic acoustic concepts. The complete data and geometry referred to in this paper are available upon request.

## VII.  ACKNOWLEDGEMENTS

## VIII.  References

[1] Hubbard, H. H., editor, Aeroacoustics of Flight Vehicles: Theory and Practice: Volume 1, NASA Reference Publication 1258, Vol 1, WRDC Technical Report 90-3052.

[2] Loew, R.A., Lauer, J.T.,  MCAllister, J., and Sutliff, D.L., "The Advanced Noise Control Fan", NASA/TM–2006-214368, also AIAA–2006-3150, Nov 2006.

[3] MCAllister, J., Loew, R.A., Lauer, J.T., and Sutliff, D.L., "The Advanced Noise Control Fan Baseline Measurements", NASA/TM–2009-215595, also AIAA–2009-0624, Oct 2009.

[4] Heidelberg, L.J., Hall, D.G., Bridges, J.E., and Nallasamy, N., "A Unique Ducted Fan Test Bed for Active Noise Control and Aeroacoustics Research", NASA TM–107213, also AIAA–96–1740.

[5] Sutliff, D.L., Nallasamy, N., and Elliott, D.M., "Baseline Acoustic Levels of the NASA Active Noise Control Fan Rig", NASA TM–107214, also AIAA–96–107214.

[6] D.L. Sutliff. "Rotating Rake Turbofan Duct Mode Measurement System", International Journal of Aeroacoustics, June 2007.

[7] Rice, Edward, J., "Spinning Mode Sound Propagation in Ducts with Acoustic Treatment", NASA TN D-7913, May 1975.

[8] Tyler, J.M and Sofrin, T.G., "Axial Flow Compressor Noise Studies", *SAE Transactions*, Vol. 70, 1962.

[9] Heidelberg, L.J., Sutliff, D.L., and Nallasamy, M., 'Azimuthal Directivity of Fan Tones Containing Multiple Modes", NASA TM-107464, AIAA 97-1587.

[10] Hall, D. G., Heidelberg, L., and Konno, K., "Acoustic Mode Measurements in the Inlet of a Model Turbofan Using a Continuously Rotating Rake: Data Collection/Analysis Techniques," AIAA Paper No. 93-0599, 1993.

[11] Cicon, D. E. and Sofrin, T. G.,"Method for Extracting Forward Acoustic Wave Components from Rotating Microphone Measurements in the Inlets of Turbofan Engines," NASA CR-195457, April 1995.